Saturable discrete vector solitons in one-dimensional photonic lattices

Rodrigo A. Vicencio,[1,2] Eugene Smirnov,[3] Christian E. Rüter,[3] Detlef Kip,[3] and Milutin Stepić[4,5]

[1]*Max Planck Institute of Physics of Complex Systems, 01187 Dresden, Germany,*
[2]*Departamento de Física, Facultad de Ciencias, Universidad de Chile, Santiago, Chile*
[3]*Institute of Physics and Physical Technologies, Clausthal University of Technology, 38678 Clausthal-Zellerfeld, Germany*
[4]*Department of Optical Technologies, National Institute of Metrology, 38116 Braunschweig, Germany,*
[5]*Vinča Institute of Nuclear Sciences, P.O.B. 522, 11001 Belgrade, Serbia*

Localized vectorial modes, with equal frequencies and mutually orthogonal polarizations, are investigated both analytically and experimentally in a one-dimensional photonic lattice with saturable nonlinearity. It is shown that these modes may span over many lattice elements and that energy transfer among the two components is both phase and intensity dependent. The transverse electrically polarized mode exhibits a single-hump structure and spreads in cascades in saturation, while the transverse magnetically polarized mode exhibits splitting into a two-hump structure. Experimentally such discrete vector solitons are observed in lithium niobate lattices for both coherent and mutually incoherent excitations.

PACS numbers: 42.65.Tg, 42.82.Et, 42.65.Sf, 63.20.Pw

Solitons or stable strongly localized nonlinear structures, which can elastically interact with linear waves and other solitons, have been studied in various systems in nature, ranging from astrophysics [1] and ocean waves [2], down to Josephson junctions [3] and nanowires [4]. These localized structures exist due to an exact balance between two or more counteracting effects such as, for example, dispersion and nonlinearity in the temporal domain [5]. In the optical domain, solitons may exist in specific materials, such as Kerr and photorefractive ones [6, 7]. On the other hand, solitons occur in different forms like incoherent, discrete, and vector solitons, which are not directly related to a particular material [5]. Vector solitons are composite structures that consist of two or more components which mutually self-trap in a nonlinear medium. Importantly, the individual components decay in isolation. The existence of vector solitons was first suggested by Manakov in 1974 [8]. Later on, vector solitons have been, for example, studied in carbon disulfide [9] and photorefractive crystals [10]. In periodic nonlinear systems, the so-called discrete solitons exist due to the balance between nonlinearity and discreteness [11]. They have been observed in diverse physical configurations such as biological systems, charge-transfer solids, Josephson junctions, micromechanical oscillator arrays, and photonic lattices. The latter have overtaken an important role in the study of nonlinear periodic systems [12, 13] due to compact setups with good control of relevant parameters like diffraction coefficients and nonlinearities. Such photonic crystals have periodic distributions of the refractive index and light propagation is associated with allowed bands and forbidden gaps, analog to propagation of electrons in crystalline lattices [14].

One-dimensional (1D) discrete vector solitons (DVS) originating from the first band have been already investigated both analytically [15, 16] and experimentally [17] in nonlinear cubic waveguide arrays (WA). The two-dimensional case was studied, too [18]. Finally, multi-band vector solitons, in which individual components stem from different bands, were also recently suggested and demonstrated [19]. The aim of the present study is to investigate DVS in media with saturable nonlinearity. Prime examples of such media are photonic lattices in photorefractive crystals. Additionally, semiconductors at higher light intensities also exhibit saturation [20]. It has been shown that saturation, which may occur in a cascade manner in discrete systems [21], is responsible for the existence of multiple zeros of the Peierls-Nabarro potential, leading to free steering of large amplitude solitons, and stable propagation of inter-site modes in 1D and 2D systems [22]. Various species of two-component saturable DVS have been investigated recently, where it was assumed that both components have the same polarization and different frequencies [23]. In what follows we are interested in the situation where the components have the same frequency but differ in polarization.

By following the procedures outlined in Refs. [10, 24], assuming only nearest neighbor interactions, and by using the slowly varying envelope approximation, one may obtain the following model equations:

$$i\frac{\partial u_n}{\partial \xi} + L_u u_n - \beta\,\frac{(u_n + s_2 B v_n)}{(1+|u_n|^2+s_1|v_n|^2)} = 0,$$
$$i\frac{\partial v_n}{\partial \xi} + L_v v_n - \beta\,\frac{(s_1 B u_n + s_3 A v_n)}{(1+|u_n|^2+s_1|v_n|^2)} = 0, \quad (1)$$

where $L_u u_n = (C_0 - \Delta k)u_n + V_0(u_{n+1} + u_{n-1})$ and $L_v v_n = [C_0 v_n + V_0(v_{n+1} + v_{n-1})]/s_1$. Here ξ is the normalized propagation coordinate (y in the experiment). The normalized envelopes u_n and v_n correspond to transverse electrically (TE) and magnetically (TM) polarized fields, respectively. The parameter β represents the nonlinear coefficient, the normalized coupling constant is denoted by V_0, Δk is the normalized difference of TE and TM wave numbers, whereas C_0 can be regarded as a normalized propagation constant. By defining birefringence $\Delta n = n_x - n_z$ and average refractive index

$n_0 = (n_x + n_z)/2$, we write the function $s_j \approx 1 + j\Delta n/n_0$. Finally, $A = r_{xxz}/r_{zzz}$ and $B = r_{xzx}/r_{zzz}$, where r_{ijk} denote the components of the Pockels tensor [10]. One may notice that in general, alike DVS in Kerr media [16–18], in our situation there exists no possibility to separate cross-phase and four-wave mixing effects. A conserved quantity of this model is the total power, $P = \sum_n \left(|u_n|^2 + s_1|v_n|^2\right) = P_u + s_1 P_v$. By using (1), it can be shown that $\partial P/\partial\xi = 0$ implies:

$$\frac{\partial P_u}{\partial \xi} = -s_1 \frac{\partial P_v}{\partial \xi} = 2\beta s_2 B \sum_n \frac{\mathrm{Im}(v_n u_n^*)}{(1 + |u_n|^2 + s_1|v_n|^2)} \,. \tag{2}$$

This expression gives us information on the energy (power) exchange among the TE and TM components which clearly will depend on the total level of power in each waveguide. By considering a one-channel constant-amplitude propagation of the form $u_0(\xi) = u_0 \exp[i(\lambda_u \xi + \phi_u)]$ and $v_0(\xi) = v_0 \exp[i(\lambda_v \xi + \phi_v)]$, where λ_i and ϕ_i correspond to the respective propagation constants and initial phases, respectively, we obtain the following expression for the power transfer: $\partial P_u/\partial\xi \sim \sin(\Delta\lambda\xi + \Delta\phi)$, where $\Delta\lambda = \lambda_v - \lambda_u$ and $\Delta\phi = \phi_v - \phi_u$. By assuming only a linear and local dependence of the propagation constants, from (1) we get: $\lambda_u \approx C_0 - \Delta k, \lambda_v \approx C_0/s_1$, which results in $\Delta\lambda \approx \Delta k$. If the components are initially in phase ($\Delta\phi = 0$), the power transfer will be initially towards the TE mode provided that $\Delta k > 0$, and towards the TM mode otherwise [16].

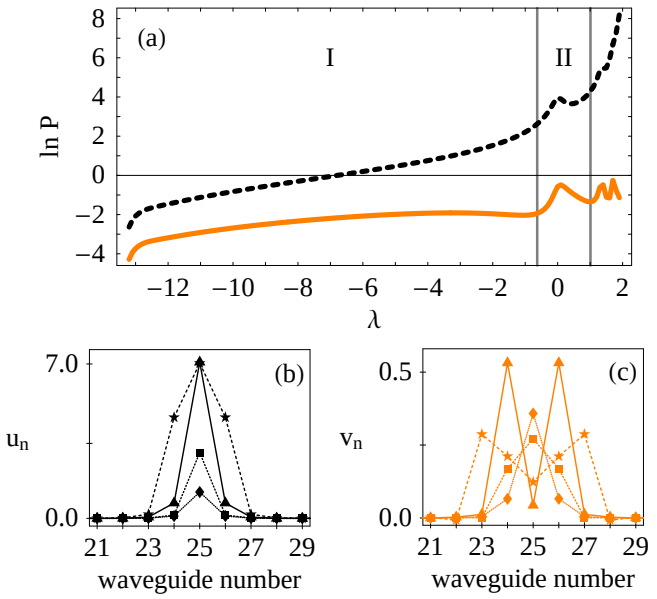

FIG. 1: (Color online). (a) TE (dashed line) and TM (continuous line) powers as a function of the propagation constant. Vertical lines separate regions. (b) and (c) TE and TM profiles, respectively: Diamonds, squares, triangles and stars correspond to $\lambda = -5, -1, 0$, and 1.1, respectively. $C_0 = \Delta k = \beta = 10$, $V_0 = 1$.

To gain a theoretical background of the model (1), we use a Newton-Raphson method to find coupled localized stationary solutions of the form: $u_n(\xi) = u_n \exp(i\lambda_u \xi)$ and $v_n(\xi) = v_n \exp(i\lambda_v \xi)$, with $u_n, v_n \in \Re$. For the sake of simplicity we assume $\lambda_u = \lambda_v \equiv \lambda$, which in turn disables the power exchange between DVS components [$\mathrm{Im}(v_n u_n^*) = 0$ in (2)]. These solutions may be regarded as the final stage of mode profiles after the DVS is formed. The power dependence of the two components on propagation constant, for the chosen set of experimentally achievable parameters [25], is shown in Fig. 1(a) in a logarithmic scale. The region of existence of localized modes is between the low-amplitude and high-amplitude limits for the upper band edge plane wave [22] of the composed system of equations (1). In the present case, this region corresponds to $\sim \lambda \in \{-13, 2\}$. Power of the TE mode always exceeds that of TM polarization and, interestingly, grows in a similar fashion as the power of the on-site mode A in Ref. [21]. For any λ, the TE mode is always a one-hump structure [see Fig. 1(b)] which spreads transversally in the region of saturation [21]. We may separate the $P\lambda$ diagram in smaller regions depending on the shape of the TM mode. In region I [$\sim \lambda \in \{-13, -0.6\}$], the TM mode corresponds to a one-hump structure [diamonds and squares in Fig. 1(c)]. In region II [$\sim \lambda \in \{-0.6, 1\}$], the TM mode corresponds to a two-hump structure separated by only one site [triangles in Fig. 1(c)]. In the next regions, the TM mode increases its distance between the two humps in an odd number of waveguides [as an example, see stars in Fig. 1(c)].

While the total power increases, local saturation takes place [22]. As $\Delta k > 0$, the TE mode is the one which gains power. Therefore the TE mode starts to increase its power locally together with the TM mode [region I in Fig. 1(a), diamonds and squares in Fig. 1(b,c)]. However, above some critical level of power [region II in Fig. 1(a), triangles in Fig. 1(b,c)] the local power in the center site is too high and the only possibility for the TM mode to exist is by exploring the neighborhood looking for a more stable configuration. Then, the TE mode further increases its power but now, due to saturation, by increasing the amplitudes in the next sites [see stars in Fig. 1(b)]. Again, the TM mode finds a new configuration which is initially stable, but now the separation between peaks consists of three sites [stars in Fig. 1(c)]. If we continue increasing the power we observe that the TE mode preserves its one-hump structure, by increasing its width, while the TM mode has a two-hump structure where the separation between peaks continuously increases. Therefore, the DVS is mostly TE polarized, except at tails which have a dominating TM polarization. The linear stability analysis of solutions coincides with the Vakhitov-Kolokolov criterion [5]: modes are stable for $\partial P/\partial\lambda > 0$, and unstable otherwise. This implies that in region I solutions are always stable and, in the

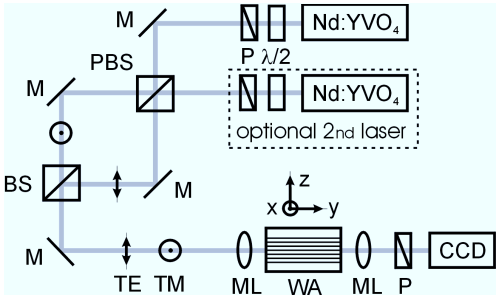

FIG. 2: Scheme of the experimental setup.

next regions, there exist both stable and unstable subregions [see Fig. 1(a)].

To verify our theoretical predictions we use the experimental setup sketched in Fig. 2. A cw laser with wavelength 532 nm is split into two orthogonally polarized (TE and TM) mutually coherent waves with the help of a polarizing beam splitter PBS. Optionally, to allow for mutually incoherent interaction of the two components, a TM polarized wave can be provided by a second laser of the same wavelength. Input power is adjusted with a combination of half wave plate $\lambda/2$ and polarizer P. The two input beams are used to excite narrow single-channel TE and TM polarized modes of the WA by using a 40× microscope lens ML. This nonlinear WA is fabricated in x-cut lithium niobate doped with copper. The length of our sample along the propagation y-direction is 11 mm and the array consists of 250 parallel titanium in-diffused waveguide channels that are 4 μm wide with a separation of 4.4 μm (grating period $\Lambda = 8.4\,\mu$m) [26]. A second microscope lens ML images the intensity on the output face onto a CCD camera, where an additional polarizer P allows for independent observation of both TE and TM components of the DVS.

The nonlinear dynamics of TE only, TM only, and both TE and TM modes (mutually coherent from the same light source) is presented in Fig. 3. Here we make use of the fact that, in photorefractives crystals, the nonlinearity grows exponentially in time, $\beta(t) = \beta\,(1-\exp[-t/\tau])$, where τ is the dielectric response time [27]. Initially, after switching on the light ($t = 0$), discrete diffraction is monitored for each situation. Although one may observe initial focusing of the TE mode within the first minutes in Fig. 3(a) (an even weaker effect is observed for TM), both modes alone are incapable to form a localized structure due to the low individual level of power [Fig. 3(a,b)] [28]. On the other hand, when both input polarizations are present [Fig. 3(c)] a very well localized five-channel DVS is formed after $t = 30$ min and does not change its shape for another two hours of observation.

Stationary images of DVS collected from the output facet of the sample for a fixed value of TE power and different values of TM power are presented in Fig. 4(a). As can be seen, the shape of the DVS slightly changes for different power ratios P_u/P_v. TE and TM polarized components for a power ratio $P_u/P_v = 1$ (steady state) are shown in Fig. 4(b). As predicted, a dominating single-hump TE polarized component and a weaker double-humped TM component are observed. The role of the TM input polarization can be further analyzed by blocking the TE input after stable formation of the DVS in Fig. 4(c). Obviously the TM polarized input light has transferred most of its energy to the TE component, forming a single-hump solution, while the remaining power is trapped in form of a two-hump solu-

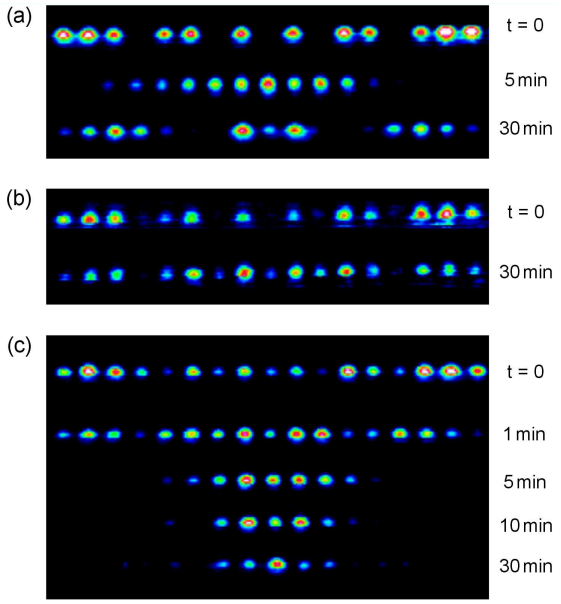

FIG. 3: (Color online). Experimentally observed DVS for mutually coherent input beams. Temporal nonlinear evolution of output intensity for (a) TE component alone ($P_u = 150\,\mu$W); (b) TM component alone ($P_v = 300\,\mu$W); and (c) both component together ($P_u = 150\,\mu$W, $P_v = 300\,\mu$W).

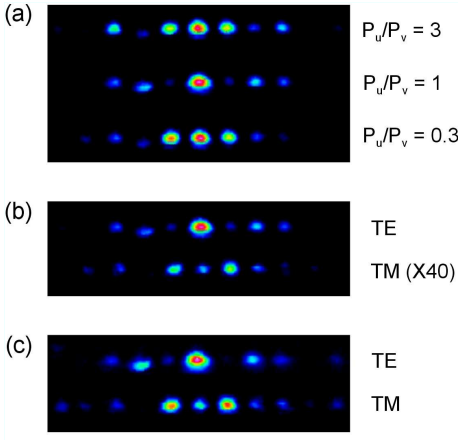

FIG. 4: (Color online). Mode analysis of stationary DVS. Stationary output intensity for (a) DVS (TE + TM) for different power ratios P_u/P_v; (b) TE and TM (amplified 40×) polarized components for $P_u/P_v = 1$; and (c) TE and TM polarized components for $P_u/P_v = 1$ immediately taken when TE beam is blocked after formation of the DVS.

tion [within several minutes, this structure decays into the one of Fig. 3(b)]. The energy transfer, from ordinary to extraordinary polarization (TM → TE), is due to a specific anisotropic nonlinearity in $LiNbO_3$ [in model (1), this corresponds to consider $\Delta k > 0$]. The mechanism of coupling of orthogonally polarized modes is explained by writing holographic gratings due to photovoltaic currents. Light is anisotropically diffracted from these shifted gratings with polarization conversion, which leads to an energy exchange among the modes [29].

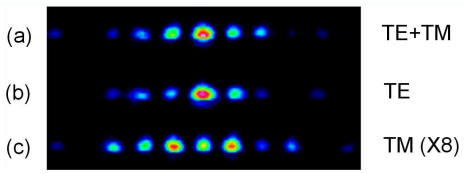

FIG. 5: (Color online). Experimentally observed DVS for mutually incoherent input beams. Stationary output intensity for (a) DVS [TE + TM] for $P_u/P_v = 1.5$; (b) TE polarized component; and (c) TM polarized components (amplified 8×).

Energy coupling of orthogonally polarized waves can be prevented by using mutually incoherent input beams ($B = 0$). Experimentally this is realized by a second laser of the same wavelength (see Fig. 2), which now provides the TM polarized input beam, and corresponding results for the steady-state DVS formation are shown in Fig. 5. Again a two-hump structure is observed for the TM component, which now guides a significant part of the total power of the soliton.

In conclusion, we suggested a rather general theoretical model to describe saturable discrete vector solitons having orthogonally polarized components. Power transfer and coupling between TE and TM components is investigated as well as the corresponding localized stationary solutions. We discovered that these composite solitons might have different width and shape depending on the region of parameters. The dominating TE mode is single-humped while the weaker TM mode may exhibit both one- and two-hump structures. We confirm our findings experimentally by using either coherent or mutually incoherent excitations, where the latter is used to suppress energy coupling in formation of discrete vector solitons. Our experimental conditions match the region II of stationary solutions, a region with an intermediate level of power and highly localized solutions. This is because the one-channel input used in the experiment excites a strongly localized region of the array with high local intensity. The results obtained here could be useful in the codification of signals, filtered by polarization, in future all-optical communication networks.

We gratefully acknowledge financial support from BMBF (grant DIP-E6.1), DFG (grant KI482/8-1), and MNZŽSRS (grant 14-1034).

[1] M. G. Abramyan, Astrophysics **22**, 288 (1985).
[2] T. P. Stanton and L. A. Ostrovsky, Geophys. Research Lett. **25**, 2695 (1998).
[3] J. Pfeiffer, M. Schuster, A.A. Abdumalikov, and A.V. Ustinov, Phys. Rev. Lett. **96**, 034103 (2006).
[4] R. El-Ganainy et al., Opt. Express **14**, 2277 (2006).
[5] Yu. S. Kivshar and G. P. Agrawal, *Optical Solitons: From Fibers to Photonic Crystals* (Academic, San Diego, 2003).
[6] A. Barthelemy, S. Maneuf, and C. Froehly, Opt. Commun. **55**, 201 (1985).
[7] M. Segev, B. Crosignani, A. Yariv, and B. Fischer, Phys. Rev. Lett. **68**, 923 (1992).
[8] S. V. Manakov, Sov. Phys. JETP **38**, 248 (1974).
[9] N. Shalaby and A. J. Barthelemy, IEEE J. Quantum Electron. **28**, 2376 (1992).
[10] M. Segev et al. Opt. Lett. **20**, 1764 (1995).
[11] D. N. Christodoulides, F. Lederer, and Y. Silberberg, Nature **424**, 817 (2003); D. K. Campbell, S. Flach, and Yu. S. Kivshar, Phys. Today **57** (1), 43 (2004).
[12] D. N. Christodoulides and R. I. Joseph, Opt. Lett. **13**, 794 (1988).
[13] H. S. Eisenberg, Y. Silberberg, R. Morandotti, A.R. Boyd, and J.S. Aitchison, Phys. Rev. Lett. **81**, 3383 (1998).
[14] J. W. Fleischer et al., Opt. Express **13**, 1780 (2005).
[15] S. Darmanyan, A. Kobyakov, E. Schmidt, and F. Lederer, Phys. Rev. E **57**, 3520 (1998).
[16] R. A. Vicencio, M. I. Molina, and Yu. S. Kivshar, Phys. Rev. E **71**, 056613 (2005); Opt. Lett. **29**, 2905 (2004).
[17] J. Meier et al., Phys. Rev. Lett. **91**, 143907 (2003).
[18] J. Hudock, P.G. Kevrekidis, B.A. Malomed, and D.N. Christodoulides, Phys. Rev. E **67**, 056618 (2003); Z. Chen et al., Opt. Lett. **29**, 1656 (2004).
[19] O. Cohen, T. Schwartz, J.W. Fleischer, M. Segev, and D.N. Christodoulides, Phys. Rev. Lett. **91**, 113901 (2003); D. Mandelik, H.S. Eisenberg, Y. Silberberg, R. Morandotti, and J.S. Aitchison, Phys. Rev. Lett. **90**, 053902 (2003).
[20] J.-L. Coutaz and M. Kull, J. Opt. Soc. Am. B **8**, 95 (1991).
[21] M. Stepić, D. Kip, Lj. Hadžievski, and A. Maluckov, Phys. Rev. E **69**, 066618 (2004).
[22] Lj. Hadžievski, A. Maluckov, M. Stepić, and D. Kip, Phys. Rev. Lett. **93**, 033901 (2004); R. A. Vicencio and M. Johansson, Phys. Rev. E **73**, 046602 (2006); E. Smirnov, C.E. Ruter, M. Stepić, D. Kip, and V. Shandarov, Phys. Rev. E **74**, 065601(R) (2006).
[23] E. P. Fitrakis, P.G. Kevrekidis, B.A. Malomed, and D.J. Frantzeskakis, Phys. Rev. E **74**, 026605 (2006).
[24] M. I. Carvalho, S.R. Singh, D.N. Christodoulides, and R.I. Joseph, Phys. Rev. E **53**, R53 (1996).
[25] In $LiNbO_3$ $A = r_{113}/r_{333} \approx 0.33$, $B = r_{131}/r_{333} \approx 1$, $\Delta n \approx 0.09$, and $n_0 \approx 2.3$.
[26] F. Chen et al., Opt. Express **13**, 4314 (2005).
[27] M. Wesner, C. Herden, R. Pankrath, D. Kip, and P. Moretti, Phys. Rev. E **64**, 036613 (2001).
[28] For slightly modified WA having either higher nonlinearity or weaker diffraction discrete solitons may be observed for TE input alone.
[29] D. Kip and E. Krätzig, Opt. Lett. **17**, 1563 (1992).